THE JOURNAL OF PHYSICAL CHEMISTRY Letters

Letter

Cite This: J. Phys. Chem. Lett. 2018, 9, 4532−4538

pubs.acs.org/JPCL

Two-Step Growth of 2D Organic−Inorganic Perovskite Microplates and Arrays for Functional Optoelectronics

Lei Li,[†,#] Junze Li,[†,#] Shangui Lan,[†] Gaoming Lin,[†] Jun Wang,[†] Haizhen Wang,[‡] Yining Xuan,[†] Hongmei Luo,[‡] and Dehui Li*,[†,§]

[†]School of Optical and Electronic Information, Huazhong University of Science and Technology, Wuhan 430074, China
[‡]Department of Chemical and Materials Engineering, New Mexico State University, Las Cruces, New Mexico 88003, United States
[§]Wuhan National Laboratory for Optoelectronics, Huazhong University of Science and Technology, Wuhan 430074, China

Supporting Information

ABSTRACT: Two-dimensional (2D) perovskites have recently attracted intensive interest for their great stability against moisture, oxygen, and illumination compared with their three-dimensional (3D) counterparts. However, their incompatibility with a typical lithography process makes it difficult to fabricate integrated device arrays and extract basic optical and electronic parameters from individual devices. Here, we develop a combination of solution synthesis and a gas−solid-phase intercalation strategy to achieve hexagonal-shaped 2D perovskite microplates and arrays for functional optoelectronics. The 2D perovskite microplates were achieved by first synthesizing the lead iodide (PbI_2) microplates from an aqueous solution and then following with intercalation via the vapor transport method. This method further allows us to synthesize arrays of 2D perovskite microplates and create individual 2D perovskite microplate-based photodetectors. In particular, chlorine (Cl) can be efficiently incorporated into the microplates, resulting in significantly improved performance of the 2D perovskite microplate-based photodetectors.

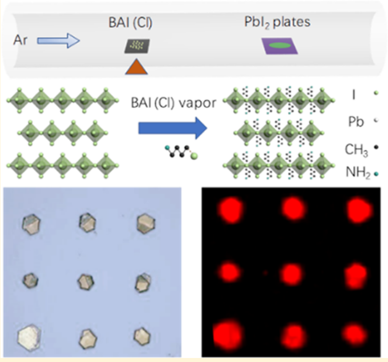

Three-dimensional (3D) organic−inorganic halide perovskites have been extensively studied in the past few years due to the unprecedented rapid surge of the power conversion efficiency of the perovskite solar cells to a certified efficiency higher than 22% within a few years[1−3] and fairly good performance of perovskite-based photodetectors,[4,5] lasers,[6,7] and light-emitting devices.[8−14] However, 3D perovskites are inherently unstable in the presence of moisture, heat, and illumination, which greatly limits the commercialization of perovskite-based optoelectronic applications.[15−19]

Recently, newly emerging 2D organic−inorganic perovskites have attracted increasing attention because of their great environmental stability compared with 3D perovskites.[20−25] The general formula of such 2D perovskites is $(RNH_3)_2A_{n-1}M_nX_{3n+1}$, where RNH_3 is a large aliphatic or aromatic alkylammonium spacer cation, A is a monovalent organic cation, M is a divalent metal cation, X is a halide anion, and n represents the number of $[MX_6]^{4-}$ octahedral structures sandwiched between two layers of spacer cations.[19,26] In 2D perovskites, the long and bulky hydrophobic spacers can prevent the $[MX_6]^{4-}$ octahedra from being directly exposed to moisture, and thus, their stability in ambient can be greatly enhanced. Previous studies reveal that the 2D perovskite-based solar cells are able to maintain 60% of their initial power conversion efficiency under illumination after 2250 h and exhibit greater moisture tolerance under 65% relative humidity (RH) compared with their 3D counterpart-based solar cells.[19] In addition to the improved stability, 2D perovskites are equipped with inherent multiple quantum well structures with an extremely large exciton binding energy and tunable quantum well thickness by simply manipulating the number n, which provides an ideal platform to investigate the exciton−polaritons and explore for novel photonic devices.[27,28] In particular, the layered nature allows us to obtain few-layer 2D perovskite sheets by mechanical exfoliation and integrate them with other 2D layered materials such as graphene and transition metal dichalcogenides (TMDs) to realize a variety of functions as demanding.[29−31]

To fully explore the potential applications of 2D perovskites, it is essential to fundamentally understand their photophysical and electronic properties and extract the basic optical and electronic parameters of the 2D perovskites.[32] Nevertheless, the photophysical and electronic properties of 2D perovskites still remain largely unexplored partially due to the difficulty of fabricating individual perovskite devices.[29] Although their stability has been greatly improved, 2D perovskites are still incompatible with a typical lithography process, and thus, most studies on 2D perovskites to date are limited to solution-processed films, which contain a great number of grains leading to extensive grain boundary scattering and trapping.[29,33] Here, we report on a synthetic strategy combining solution synthesis

Received: June 14, 2018
Accepted: July 27, 2018
Published: July 27, 2018

DOI: 10.1021/acs.jpclett.8b01861
J. Phys. Chem. Lett. 2018, 9, 4532−4538

and gas−solid-phase intercalation to precisely grow 2D perovskite microplates onto the desired positions.[32] This simple method enables us to fabricate individual 2D perovskite electronic devices as well as scalable arrays of 2D perovskites for further integrated device arrays with excellent quality.[33] In particular, the two-step method also allows us to efficiently incorporate chloride into the 2D perovskites $(BA)_2PbI_4$ with a relatively high ratio to improve the device performance, while it has been revealed that the ratio of Cl incorporation (doping) in an iodide-based 3D perovskite cannot be very high (less than 3−4%).[34]

Figure 1a displays schematic illustrations of the experimental setup and the corresponding crystal structure changes for the gas−solid-phase intercalation process. The entire intercalation process was completed in a home-built vapor transport chemical vapor deposition system. The PbI_2 microplates were first grown on the substrates either by directly dropping a saturated PbI_2 aqueous solution or via a pattern growth method reported previously (see the Methods section).[33,35] The as-grown PbI_2 microplates were then placed downstream of the quartz tube, while the butylammonium iodide (BAI) or butylammonium chloride (BACl) powder was placed at the center of the tube furnace. After heating the quartz tube to 150 (120) °C and maintaining this temperature for 2 h (30 min), the PbI_2 microplates were successfully converted into $(BA)_2PbI_4$ ($(BA)_2PbI_{4-x}Cl_x$) plates, respectively. During the intercalation process, one layer of $[PbI_6]^{4-}$ octahedra was sandwiched by two layers of BAI (BACl) molecules, leading to the formation of 2D perovskite $(BA)_2PbI_4$ ($(BA)_2PbI_{4-x}Cl_x$), as shown in Figure 1a.

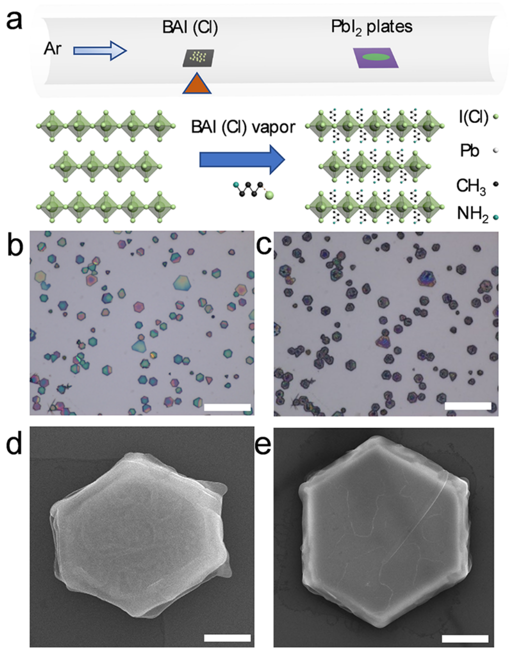

Figure 1. (a) Setup and corresponding crystal structure changes for the gas−solid-phase intercalation process. (b,c) Optical images of as-grown PbI_2 microplates (b) and corresponding converted $(BA)_2PbI_{4-x}Cl_x$ microplates (c). The scale bar is 100 μm. (d,e) SEM images of the individual converted $(BA)_2PbI_4$ (d) and $(BA)_2PbI_{4-x}Cl_x$ (e). The scale bar is 20 μm.

Previous studies on 3D perovskites have demonstrated that Cl doping into $CH_3NH_3PbI_3$ (denoted as $MAPbI_3$) can dramatically improve the performance of $MAPbI_3$-based optoelectronic devices without substantially changing the band gap even if the ratio of Cl incorporation in $MAPbI_3$ is very low.[34,36] It has also been revealed that the Cl doping concentration cannot surpass 3−4% in $MAPbI_3$ from theoretical aspects and Cl atoms preferentially occupy the apical positions of $[PbI_6]^{4-}$ octahedra in $MAPbI_3$.[34] Due to the layer nature of 2D perovskites where it is easier for Cl atoms to replace the I atoms at the apical positions of $[PbI_6]^{4-}$ octahedra, we anticipate that the ratio of Cl incorporation in 2D perovskites might be much larger than that in $MAPbI_3$. Thus, we also used BACl powder as the intercalation source to verify this hypothesis and to check the effect of Cl doping on the morphology and device performance of 2D perovskites.

Figure 1b,c exhibits optical images of the PbI_2 microplates and converted 2D perovskites by using BACl as the intercalation source, respectively. The converted microplates largely maintain a similar hexagonal shape with a striking color contrast compared with PbI_2 microplates (Figure 1b). While the shape of the converted microplates slightly deviates from the hexagonal shape of PbI_2 microplates due to phase transition from the hexagonal structure of PbI_2 to the orthorhombic structure of 2D perovskites, the striking color change before and after intercalation can be ascribed to the significant increase of the thickness of $(BA)_2PbI_{4-x}Cl_x$ after insertion of BACl molecules and the slightly rough surface of $(BA)_2PbI_{4-x}Cl_x$ microplates. The energy dispersive spectrum (EDS) suggests that the atomic ratio of Cl to I is close to 1:1, agreeing with the hypothesis that a much higher Cl incorporation ratio could be achieved in 2D perovskites (Supporting Information Figure S1). Similarly, $(BA)_2PbI_4$ plates have been successfully synthesized by the same synthesis procedure using BAI as the precursor source. We further take the scanning electron microscopy (SEM) images to closely inspect the surface morphology, which indicates that the surface of the converted microplates is rather smooth for intercalation with both BAI and BACl powder sources (Figure 1d,e). Nevertheless, microplates intercalated with BACl powder show a much smoother surface than that intercalated with BAI, similar to that in the 3D $MAPbI_3$ case.[34] The intercalation of PbI_2 plates in 3D perovskites needs to transfer from the hexagonal phase (PbI_2) to tetragonal phase (3D perovskites), in which case the PbI_2 microplates would break into a number of pieces (polycrystals) and thus result in a relatively rough surface after interaction. In contrast, in 2D perovskites, we expect that the weak van der Waals interaction between the $[MX_6]^{4-}$ octahedral sheets and organic spacer layers can effectively prevent the entire layer from being broken into a few pieces and thus leave excellent smooth surfaces and crystalline quality after conversion.

To further confirm that PbI_2 microplates have been completely converted to 2D perovskites and the crystalline quality of the converted 2D perovskites, we carried out XRD diffraction and temperature-dependent microphotoluminescence (PL) measurements of individual microplates. XRD patterns of the converted 2D perovskite show that the diffraction peaks of PbI_2 completely disappeared, and all diffraction peaks can be indexed to $(BA)_2PbI_4$ when BAI powder was used as the source, suggesting the complete conversion of PbI_2 microplates. For comparison, the XRD pattern of the PbI_2 microplate before intercalation is also displayed in Figure 2a. When BACl powder was used as the source, the diffraction peaks shifted to the smaller angles, and

DOI: 10.1021/acs.jpclett.8b01861
J. Phys. Chem. Lett. 2018, 9, 4532−4538

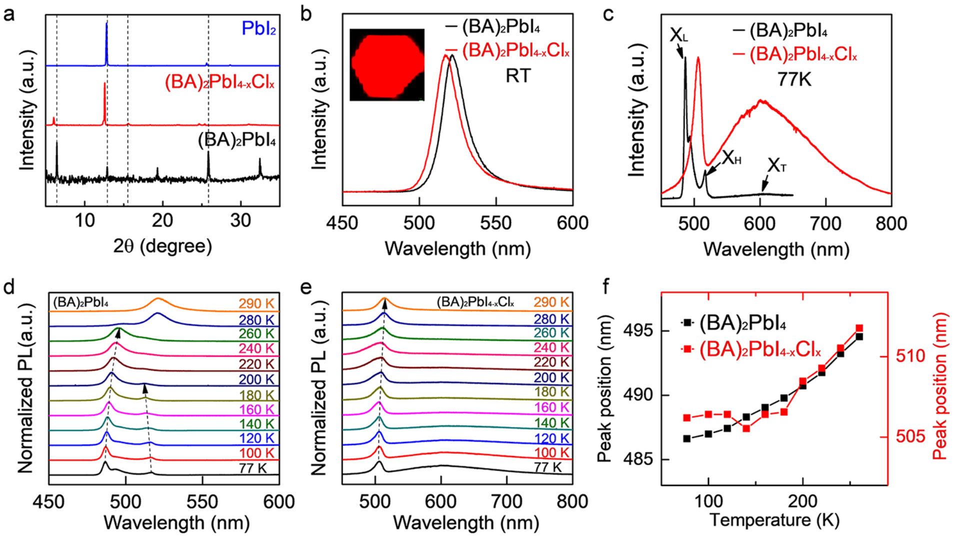

Figure 2. (a) XRD patterns of the converted $(BA)_2PbI_4$ and $(BA)_2PbI_{4-x}Cl_x$ microplates. For comparison, the XRD pattern of the PbI_2 microplate before intercalation is given as well. (b,c) Normalized room-temperature (b) and 77 K (c) PL spectra of the individual converted $(BA)_2PbI_4$ and $(BA)_2PbI_{4-x}Cl_x$ microplates. Inset in (b): PL mapping of an individual converted $(BA)_2PbI_{4-x}Cl_x$ microplate. (d,e) Temperature-dependent normalized PL of $(BA)_2PbI_4$ (d) and $(BA)_2PbI_{4-x}Cl_x$ (e) microplates from 77 to 290 K. (f) Extracted higher-energy peak position of PL spectra in (d) and (e) versus temperature.

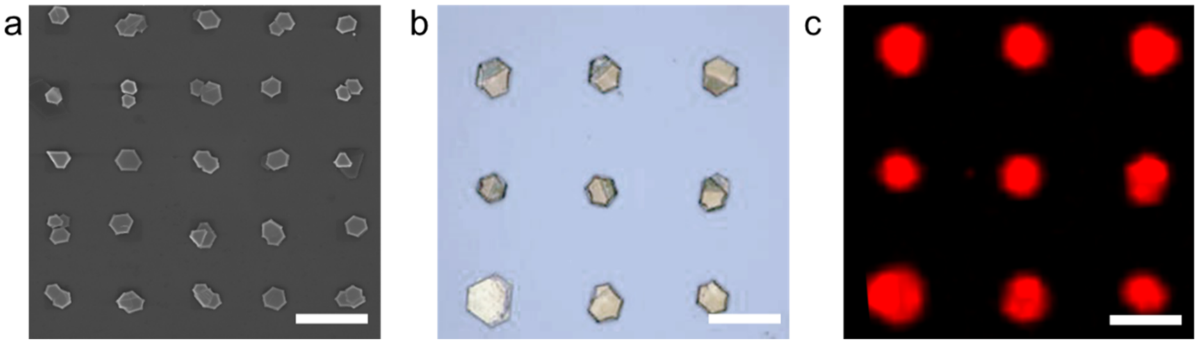

Figure 3. (a) SEM image of the converted $(BA)_2PbI_{4-x}Cl_x$ microplate array. The scale bar is 50 μm. (b,c) Optical image of the converted $(BA)_2PbI_{4-x}Cl_x$ array (b) and corresponding PL mapping (c). The scale bar is 20 μm.

some diffraction peaks cannot be indexed to $(BA)_2PbI_4$, which might originate from Cl atom-induced lattice distortion, consistent with previous reports.[24] Especially, the diffraction peak in the small-angle range (<10°) unambiguously confirms the formation of 2D perovskite (Figure 2a). Nevertheless, room-temperature PL spectra indicate that the emission intensity for both $(BA)_2PbI_4$ and $(BA)_2PbI_{4-x}Cl_x$ is more than 100 times stronger than that of PbI_2 microplates,[37] further verifying conversion of the PbI_2 (Figure 2b). PL mapping (inset of Figure 2b) also shows strong emission from the entire microplates, suggesting that the PbI_2 microplates have been completely converted with excellent uniformity. To further check whether there is a remnant PbI_2 underlayer, we grew $(BA)_2PbI_{4-x}Cl_x$microplates on a quartz substrate and measured PL spectra from both the top and bottom surface of the converted microplates. A similar PL profile from the top and bottom surfaces was observed, suggesting full conversion of PbI_2 (Supporting Information Figure S2). The slight emission peak position difference between $(BA)_2PbI_4$ and $(BA)_2PbI_{4-x}Cl_x$ might be due to Cl doping or the thickness difference of the measured microplates, which has been observed in 2D perovskites and other nanostructures.[19]

To check how the Cl doping changes the emission properties, we collected PL spectra at 77 K for both $(BA)_2PbI_4$ and $(BA)_2PbI_{4-x}Cl_x$ (Figure 2c). For $(BA)_2PbI_4$ microplates, three emission peaks are present, which can be ascribed to the low-temperature phase (X_L), high-temperature phase (X_H), and self-trapped states (X_T) according to a previous report.[38] In contrast, there are only two emission peaks for $(BA)_2PbI_{4-x}Cl_x$ microplates. According to previous studies, the higher-energy peak might be due to the free exciton emission, and the low-energy one may be due to the self-trapped exciton emission;[34] alternatively, both may originate from the self-trapped states.[24] Nonetheless, further investigations are required to clarify this.

Temperature-dependent PL studies were further carried out to confirm the conversion of PbI_2 and the crystalline quality of the converted $(BA)_2PbI_4$ and $(BA)_2PbI_{4-x}Cl_x$ microplates. Only three emission peaks were observed at low temperatures, consistent with the solution-processed $(BA)_2PbI_4$ without any defect emission,[31,39] while a sudden emission peak shift occurs at around 260 K, indicating a phase transition,[40,41] both of which show that the converted $(BA)_2PbI_4$ has excellent crystalline quality (Figure 2d). The extracted energy for the higher-energy peak versus temperature exhibits a negative

DOI: 10.1021/acs.jpclett.8b01861
J. Phys. Chem. Lett. 2018, 9, 4532−4538

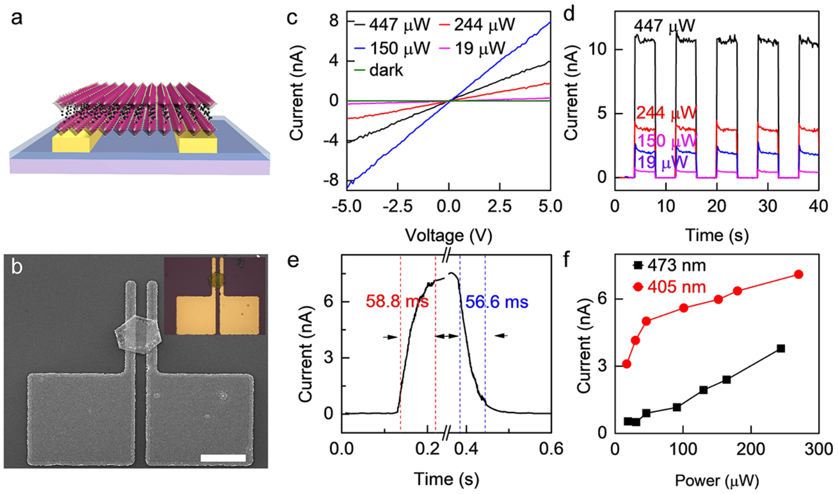

Figure 4. (a,b) Schematic illustration (a) and SEM image (b) of the converted individual $(BA)_2PbI_4$ device. Inset: optical image of the two-probe device. The scale bar is 20 μm. (c) Current−voltage curves of the individual microplate device in the dark and under 473 nm defocused laser illumination with different powers. (d) Optical switch characteristic of the individual microplate device under a bias of 5 V. (e) Temporal photocurrent response excited by a 473 nm laser with a power of 447 μW under a bias of 5 V. (f) Photocurrent versus incident light power under 405 and 473 nm laser illumination at a bias of 5 V.

temperature coefficient, agreeing with the solution-processed $(BA)_2PbI_4$ as well (Figure 2f). For the PL spectra of $(BA)_2PbI_{4-x}Cl_x$ plates, a similar temperature-dependent emission energy and no phase transition have been observed in the temperature range that we investigated due to the Cl doping (Figure 2e,f). Overall, the low-temperature PL spectra, phase transition, and temperature-dependent PL emission energy all support that the PbI_2 microplates have completely converted to $(BA)_2PbI_4$ or $(BA)_2PbI_{4-x}Cl_x$ with excellent crystalline quality.

This two-step growth method also allows us to synthesize large arrays of 2D perovskite crystals for integrated electronic and optoelectronic systems. To achieve this, we first grow the arrays of PbI_2 from an aqueous solution by functionaling the substrates and then convert the PbI_2 arrays to arrays of 2D perovskites via interaction with BAI or BACl powder in a vapor transport chemical vapor deposition system. 2D perovskite arrays with controllable physical dimensions, spatial location, and various lattice arrangements on diverse substrates could be achieved using this synthetic strategy with great flexibility. As a demonstration, we have successfully obtained arrays of $(BA)_2PbI_{4-x}Cl_x$ microplates with a square lattice arrangement on a SiO_2/Si substrate (Figure 3a). SEM, optical microscopy, and PL mapping images (Figure 3a−c) of the intercalated microplates indicate that the resultant array maintains the square lattice arrangement and the individual plate retains the hexagonal shape with a smooth and clear surface, suggesting the great uniformity of the converted 2D perovskite array.

With this two-step approach, we further fabricated individual 2D perovskite-based electronic devices via first selectively growing the PbI_2 plates on predefined electrodes without adopting typical lithography processes to investigate the optoelectronic properties of the 2D perovskites.[33] Figure 4a,b displays a schematic illustration, SEM, and optical images of a typical two-probe $(BA)_2PbI_4$ microplate device with a channel length of 10 μm. The nearly zero dark current of the converted $(BA)_2PbI_4$ device suggests the high-crystalline quality of our converted $(BA)_2PbI_4$ microplates with a few defects (dopants) leading to the lack of the intrinsic charge carriers (Figure 4c). Under illumination (a 473 nm laser), the photocurrent rapidly increases with the increase of the incident power, indicating the excellent photoresponse of our converted $(BA)_2PbI_4$ microplates. The nearly linear and symmetric current−voltage curves under light illumination show that the contact is close to Ohmic contact with a negligible barrier. The optical switch characteristic reveals that our converted microplate devices have excellent reversibility and stability with a low dark current of ∼10 pA and a photocurrent-to-dark ratio up to 10^3 (Figure 4d), both of which are comparable to or even better than those of previously reported solution-processed 2D perovskite photodetectors. The response speed, characterized by rising and falling time, is evaluated to be around 60 ms, also faster than that of the solution-processed 2D perovskite photodetectors.[29] The photocurrent increases sublinearly with the increase of the incident power for both 405 and 473 nm laser illumination, which might be due to the complex photogenerated carrier dynamics in semiconductors (Figure 4f). The large photocurrent difference between the 405 and 473 nm laser illumination is due to the large difference of the absorbance. The thickness of the microplates that we used is around 100 nm or below; thus, the incident light cannot be totally absorbed for such thin devices. The absorption coefficient at 405 nm is much larger than that at 473 nm,[42] leading to the much larger photocurrent for 405 nm illumination.

To check the effect of Cl doping on the optoelectronic properties of 2D perovskite devices, we fabricated $(BA)_2PbI_{4-x}Cl_x$ microplate devices and measured their photoresponse using the same procedure as that of $(BA)_2PbI_4$ devices. The current−voltage curves in the dark and under illumination indicate the fairly good contact and significant photoresponse of the $(BA)_2PbI_{4-x}Cl_x$ microplate devices (Figure 5a). The excellent reversibility and stability have also been confirmed by the optical switch characteristic (Figure 5b). With incorporation of the Cl element, the photocurrent significantly increases from 6 to around 300 nA under the same illumination condition and the same applied bias but maintains a low dark current of 10 pA (similar as that of $(BA)_2PbI_4$), corresponding to a very high on−off ratio of 10^5 (Figure 5b). Strikingly, the response speed also greatly increases from

DOI: 10.1021/acs.jpclett.8b01861
J. Phys. Chem. Lett. 2018, 9, 4532−4538

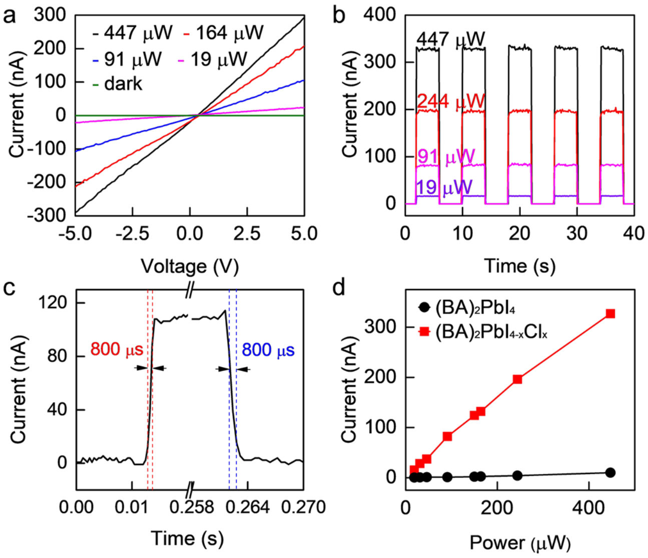

Figure 5. (a) Current−voltage curves of the individual $(BA)_2PbI_{4-x}Cl_x$ microplate device in the dark and under 473 nm defocused laser illumination with different powers. (b) Optical switch characteristic of the individual microplate device under a bias of 5 V. (c) Temporal photocurrent response excited by a 473 nm laser with a power of 91 μW under a bias of 5 V. (d) Photocurrent versus incident light power under 473 nm laser illumination at a bias of 5 V. For comparison, we also show the photocurrent versus incident light power for the $(BA)_2PbI_4$ microplate device taken from Figure 4f.

around 60 ms in $(BA)_2PbI_4$ microplate devices to around 800 μs in $(BA)_2PbI_{4-x}Cl_x$ devices (Figure 5c). A similar power-dependent photocurrent has been observed in $(BA)_2PbI_{4-x}Cl_x$ devices but with a much higher photocurrent (Figure 5d). The improved device performance with Cl doping might originate from the smoother surface and enhanced charge transport, the same as that in 3D $MAPbI_3$ films.[34] Overall, the two-step synthetic method enables us to efficiently and easily incorporate the Cl element with a much higher doping ratio than that in 3D $MAPbI_3$ films and without introducing a large number of defects to improve the performance of the iodide-based perovskite-based electronic and optoelectronic applications.

In summary, we have developed a two-step synthetic method combining solution synthesis and gas−solid-phase intercalation to controllably grow 2D perovskite microplates and arrays of 2D perovskites. XRD, SEM, and low-temperature PL studies confirm the successful formation of the 2D perovskite microplates and microplate arrays with a hexagonal shape, smooth surface, and excellent crystalline quality. We further show that this two-step method allows us to selectively grow 2D perovskite microplates on predefined electrodes to create individual 2D perovskite plate-based photodetectors and enables us to efficiently dope the Cl element at a high ratio to significantly improve the performance of the photodetectors. Our findings provide a simple synthetic method with great simplicity not only to create electronic devices based on individual 2D perovskite crystals for further investigation of their electronic and optoelectronic properties but also to synthesize 2D perovskite crystal arrays for integrated electronic devices. In particular, the gas−solid intercalation allows us to improve the performance of the 2D perovskite-based photodetectors, which opens an avenue to increase the ratio of Cl incorporation in perovskite materials.

■ METHODS

Fabrication of the Patterned Substrate. The patterned substrate has been prepared using a method reported previously. In detail, the precleaned SiO_2/Si wafer was immersed in hexamethyldisilazane (HMDS) vapor for 10 min and then rinsed with acetone for 30 s to form a self-assembled HMDS hydrophobic monolayer on the substrate surface. A photolithography process together with oxygen plasma treatment was used to selectively remove HMDS from designated/specific locations to obtain periodic arrays of hydrophilic regions. Then, the photoresist was removed by dipping the substrate into acetone for 5 min. The freshly prepared patterned substrate was further used for growth of the PbI_2 microplate array.[33]

Growth of PbI_2 Microplate Arrays. To obtain PbI_2 microplates, a saturated PbI_2 aqueous solution (0.1 g/100 mL) prepared at 80 °C was dropped onto the substrate and dried at 60 °C. The PbI_2 microplates with hexagonal shape could then randomly form on the substrate for further intercalation. For the growth of PbI_2 arrays, both the patterned substrate and aqueous solution of PbI_2 were first heated to 80 °C, and then, the heated patterned substrate was immersed in the hot saturated PbI_2 aqueous solution for 10 min. The PbI_2 microplate array grew onto the substrate after the substrate was blown to dry by Ar gas.

Conversion of PbI_2 Microplates into Perovskite Crystals. Butylammonium iodide (BAI) and butylammonium chloride (BACl) powder were synthesized using a previously reported solution method.[23,43] The BAI (BACl) powder was placed at the center of a 1 in. tube furnace, while the substrates with PbI_2 microplates were placed around 6 cm (8 cm) downstream. The tube furnace was first pumped by a mechanical pump and purged with argon (Ar) for a few minutes to completely remove the air in the quartz tube. The intercalation was conducted by heating the furnace to 150 °C (120 °C) and remaining at this temperature for 2 h (30 min) at a pressure of 8 Torr with 100 sccm of Ar gas used as the carrier gas. Finally, the furnace tube was naturally cooled down to room temperature.

Material Characterizations. Powder X-ray spectrum measurements were collected using a Bruker D2 PHPSER (Cu Kα λ = 0.15419 nm, nickel filter, 25 kV, 40 mA). Optical microscopy images were acquired by the Olympus BX53 M system microscope. The scanning electron microscopy images were collected on a JEOL 7001F field emission scanning electron microscope. The PL spectra were measured in backscattering configuration using a Horiba HR550 system equipped with a 600 g/mm grating excited by a 473 nm solid-state laser with a power of 1 μW. A liquid nitrogen continuous flow cryostat (Cryo Industry of America, U.S.A.) was used to provide continuous temperature variation from 77 to 290 K.

Photoconductivity Spectroscopy. The photocurrent measurements were carried out on a home-built setup using a two-probe configuration. The Cr/Au (10/50 nm) electrodes were first defined by photolithography followed by thermal evaporation and a lift-off process. Then PbI_2 microplates were grown on the predefined electrodes and then converted to the 2D perovskite microplates. A 405 or 473 nm solid-state laser was used to illuminate the devices. The photocurrent of the two-probe device was collected by a lock-in amplifier (Stanford SR830) coupled with a mechanical chopper. The response speed of the photodetectors was acquired using a digital oscilloscope (Tektronix MDO3032).

■ ASSOCIATED CONTENT

Ⓢ Supporting Information

The Supporting Information is available free of charge on the ACS Publications website at DOI: 10.1021/acs.jpclett.8b01861.

EDS of the individual converted $(BA)_2PbI_4$ and $(BA)_2PbI_{4-x}Cl_x$ and PL spectra acquired from both the top and bottom of converted microplates on the quartz substrate (PDF)

■ AUTHOR INFORMATION

Corresponding Author

*E-mail: dehuili@hust.edu.cn.

ORCID

Hongmei Luo: 0000-0002-9546-761X

Dehui Li: 0000-0002-5945-220X

Author Contributions

#L.L and J.L. contributed to this work equally.

Notes

The authors declare no competing financial interest.

■ ACKNOWLEDGMENTS

D.L. acknowledges support from the NSFC (61674060) and the Fundamental Research Funds for the Central Universities, HUST (2017KFYXJJ030, 2017KFXKJC003, 2017KFXKJC002, 2018KFYXKJC016) and the National Young 1000 Talent Plan of China; H.L. is grateful for support from New Mexico EPSCoR with NSF-1301346.

■ REFERENCES

(1) Saliba, M.; Matsui, T.; Domanski, K.; Seo, J. Y.; Ummadisingu, A.; Zakeeruddin, S. M.; Correa-Baena, J. P.; Tress, W. R.; Abate, A.; Hagfeldt, A.; et al. Incorporation of Rubidium Cations into Perovskite Solar Cells Improves Photovoltaic Performance. *Science* **2016**, *354*, 206−209.

(2) Green, M. A.; Ho-Baillie, A.; Snaith, H. J. The Emergence of Perovskite Solar Cells. *Nat. Photonics* **2014**, *8*, 506−514.

(3) Nie, W. Y.; Tsai, H. H.; Asadpour, R.; Blancon, J. C.; Neukirch, A. J.; Gupta, G.; Crochet, J. J.; Chhowalla, M.; Tretiak, S.; Alam, M. A.; et al. High-efficiency Solution-Processed Perovskite Solar Cells with Millimeter-Scale Grains. *Science* **2015**, *347*, 522−525.

(4) Li, W.; Wang, Z.; Deschler, F.; Gao, S.; Friend, R. H.; Cheetham, A. K. Chemically Diverse and Multifunctional Hybrid Organic−Inorganic Perovskites. *Nat. Rev. Mater.* **2017**, *2*, 16099.

(5) Wei, W.; Zhang, Y.; Xu, Q.; Wei, H. T.; Fang, Y. J.; Wang, Q.; Deng, Y. H.; Li, T.; Gruverman, A.; Cao, L.; et al. Monolithic Integration of Hybrid Perovskite Single Crystals with Heterogenous Substrate for Highly Sensitive X-Ray Imaging. *Nat. Photonics* **2017**, *11*, 315−321.

(6) Xing, G. C.; Mathews, N.; Lim, S. S.; Yantara, N.; Liu, X. F.; Sabba, D.; Gratzel, M.; Mhaisalkar, S.; Sum, T. C. Low-Temperature Solution-Processed Wavelength-Tunable Perovskites for Lasing. *Nat. Mater.* **2014**, *13*, 476−480.

(7) Li, X.; Wang, Y.; Sun, H.; Zeng, H. Amino-Mediated Anchoring Perovskite Quantum Dots for Stable and Low-Threshold Random Lasing. *Adv. Mater.* **2017**, *29*, 1701185.

(8) Xiao, Z.; Kerner, R. A.; Zhao, L.; Tran, N. L.; Lee, K. M.; Koh, T.-W.; Scholes, G. D.; Rand, B. P. Efficient Perovskite Light-Emitting Diodes Featuring Nanometre-Sized Crystallites. *Nat. Photonics* **2017**, *11*, 108−115.

(9) Wang, N.; Cheng, L.; Ge, R.; Zhang, S.; Miao, Y.; Zou, W.; Yi, C.; Sun, Y.; Cao, Y.; Yang, R.; et al. Perovskite Light-Emitting Diodes Based on Solution-Processed Self-Organized Multiple Quantum Wells. *Nat. Photonics* **2016**, *10*, 699−704.

(10) Quan, L. N.; Zhao, Y. B. A.; Garcia de Arquer, F. P.; Sabatini, R.; Walters, G.; Voznyy, O.; Comin, R.; Li, Y. Y.; Fan, J. Z.; Tan, H. R.; et al. Tailoring the Energy Landscape in Quasi-2D Halide Perovskites Enables Efficient Green-Light Emission. *Nano Lett.* **2017**, *17*, 3701−3709.

(11) Tian, W.; Zhou, H.; Li, L. Hybrid Organic-Inorganic Perovskite Photodetectors. *Small* **2017**, *13*, 1702107.

(12) Cho, H. C.; Jeong, S. H.; Park, M. H.; Kim, Y. H.; Wolf, C.; Lee, C. L.; Heo, J. H.; Sadhanala, A.; Myoung, N.; Yoo, S.; et al. Overcoming the Electroluminescence Efficiency Limitations of Perovskite Light-Emitting Diodes. *Science* **2015**, *350*, 1222−1225.

(13) Kim, Y. H.; Cho, H.; Lee, T. W. Metal Halide Perovskite Light Emitters. *Proc. Natl. Acad. Sci. U. S. A.* **2016**, *113*, 11694−11702.

(14) Cho, H.; Kim, Y. H.; Wolf, C.; Lee, H. D.; Lee, T. W. Improving the Stability of Metal Halide Perovskite Materials and Light-Emitting Diodes. *Adv. Mater.* **2018**, 1704587.

(15) Li, X.; Dar, M. I.; Yi, C. Y.; Luo, J. S.; Tschumi, M.; Zakeeruddin, S. M.; Nazeeruddin, M. K.; Han, H. W.; Gratzel, M. Improved Performance and Stability of Perovskite Solar Cells by Crystal Crosslinking with Alkylphosphonic Acid Omega-Ammonium Chlorides. *Nat. Chem.* **2015**, *7*, 703−711.

(16) Rong, Y.; Liu, L.; Mei, A.; Li, X.; Han, H. Beyond Efficiency: The Challenge of Stability in Mesoscopic Perovskite Solar Cells. *Adv. Energy Mater.* **2015**, *5*, 1501066.

(17) Wang, Z.; Shi, Z.; Li, T.; Chen, Y.; Huang, W. Stability of Perovskite Solar Cells: A Prospective on the Substitution of the A Cation and X Anion. *Angew. Chem., Int. Ed.* **2017**, *56*, 1190−1212.

(18) Chiang, C. H.; Nazeeruddin, M. K.; Gratzel, M.; Wu, C. G. The Synergistic Effect of H_2O and DMF towards Stable and 20% Efficiency Inverted Perovskite Solar Cells. *Energy Environ. Sci.* **2017**, *10*, 808−817.

(19) Chen, Y.; Sun, Y.; Peng, J.; Tang, J.; Zheng, K.; Liang, Z. 2D Ruddlesden-Popper Perovskites for Optoelectronics. *Adv. Mater.* **2018**, *30*, 1703487.

(20) Smith, I. C.; Hoke, E. T.; Solis-Ibarra, D.; McGehee, M. D.; Karunadasa, H. I. A Layered Hybrid Perovskite Solar-Cell Absorber with Enhanced Moisture Stability. *Angew. Chem., Int. Ed.* **2014**, *53*, 11232−11235.

(21) Pedesseau, L.; Sapori, D.; Traore, B.; Robles, R.; Fang, H. H.; Loi, M. A.; Tsai, H.; Nie, W.; Blancon, J. C.; Neukirch, A.; et al. Advances and Promises of Layered Halide Hybrid Perovskite Semiconductors. *ACS Nano* **2016**, *10*, 9776−9786.

(22) Cao, D. H.; Stoumpos, C. C.; Farha, O. K.; Hupp, J. T.; Kanatzidis, M. G. 2D Homologous Perovskites as Light-Absorbing Materials for Solar Cell Applications. *J. Am. Chem. Soc.* **2015**, *137*, 7843−7850.

(23) Stoumpos, C. C.; Cao, D. H.; Clark, D. J.; Young, J.; Rondinelli, J. M.; Jang, J. I.; Hupp, J. T.; Kanatzidis, M. G. Ruddlesden−Popper Hybrid Lead Iodide Perovskite 2D Homologous Semiconductors. *Chem. Mater.* **2016**, *28*, 2852−2867.

(24) Dou, L. T.; Wong, A. B.; Yu, Y.; Lai, M. L.; Kornienko, N.; Eaton, S. W.; Fu, A.; Bischak, C. G.; Ma, J.; Ding, T. N.; et al. Atomically Thin Two-Dimensional Organic-Inorganic Hybrid Perovskites. *Science* **2015**, *349*, 1518−1521.

(25) Tsai, H.; Nie, W.; Blancon, J. C.; Stoumpos, C. C.; Asadpour, R.; Harutyunyan, B.; Neukirch, A. J.; Verduzco, R.; Crochet, J. J.; Tretiak, S.; et al. High-Efficiency Two-Dimensional Ruddlesden-Popper Perovskite Solar Cells. *Nature* **2016**, *536*, 312−316.

(26) Hong, X.; Ishihara, T.; Nurmikko, A. V. Dielectric Confinement Effect on Excitons in PbI_4-Based Layered Semiconductors. *Phys. Rev. B: Condens. Matter Mater. Phys.* **1992**, *45*, 6961−6964.

(27) Wang, J.; Li, J.; Tan, Q.; Li, L.; Zhang, J.; Zang, J.; Tan, P.; Zhang, J.; Li, D. Controllable Synthesis of Two-Dimensional Ruddlesden-Popper-Type Perovskite Heterostructures. *J. Phys. Chem. Lett.* **2017**, *8*, 6211−6219.

(28) Kitazawa, N.; Ito, T.; Sakasegawa, D.; Watanabe, Y. Excitons in Self-Organized Layered Perovskite Films Prepared by the Two-Step Growth Process. *Thin Solid Films* **2006**, *500*, 133−137.

(29) Tan, Z.; Wu, Y.; Hong, H.; Yin, J.; Zhang, J.; Lin, L.; Wang, M.; Sun, X.; Sun, L.; Huang, Y.; et al. Two-Dimensional $(C_4H_9NH_3)_2PbBr_4$ Perovskite Crystals for High-Performance Photodetector. *J. Am. Chem. Soc.* **2016**, *138*, 16612−16615.

(30) Cheng, H. C.; Wang, G.; Li, D.; He, Q.; Yin, A.; Liu, Y.; Wu, H.; Ding, M.; Huang, Y.; Duan, X. Van der Waals Heterojunction Devices Based on Organohalide Perovskites and Two-Dimensional Materials. *Nano Lett.* **2016**, *16*, 367−373.

(31) Li, J.; Wang, J.; Zhang, Y.; Wang, H.; Lin, G.; Xiong, X.; Zhou, W.; Luo, H.; Li, D. Fabrication of Single Phase 2D Homologous Perovskite Microplates by Mechanical Exfoliation. *2D Mater.* **2018**, *5*, 021001.

(32) Kitazawa, N.; Yaemponga, D.; Aono, M.; Watanabe, Y. Optical Properties of Organic−Inorganic Hybrid Films Prepared by the Two-Step Growth Process. *J. Lumin.* **2009**, *129*, 1036−1041.

(33) Wang, G. M.; Li, D. H.; Cheng, H. C.; Li, Y. J.; Chen, C. Y.; Yin, A. X.; Zhao, Z. P.; Lin, Z. Y.; Wu, H.; He, Q. Y.; et al. Wafer-Scale Growth of Large Arrays of Perovskite Microplate Crystals for Functional Electronics and Optoelectronics. *Sci. Adv.* **2015**, *1*, e1500613.

(34) Colella, S.; Mosconi, E.; Fedeli, P.; Listorti, A.; Gazza, F.; Orlandi, F.; Ferro, P.; Besagni, T.; Rizzo, A.; Calestani, G.; et al. $MAPbI_{3-x}Cl_x$ Mixed Halide Perovskite for Hybrid Solar Cells: The Role of Chloride as Dopant on the Transport and Structural Properties. *Chem. Mater.* **2013**, *25*, 4613−4618.

(35) Heo, J. H.; Im, S. H.; Noh, J. H.; Mandal, T. N.; Lim, C.-S.; Chang, J. A.; Lee, Y. H.; Kim, H.-j.; Sarkar, A.; Nazeeruddin, M. K.; et al. Efficient Inorganic−Organic Hybrid Heterojunction Solar Cells Containing Perovskite Compound and Polymeric Hole Conductors. *Nat. Photonics* **2013**, *7*, 486−491.

(36) Mosconi, E.; Amat, A.; Nazeeruddin, M. K.; Grätzel, M.; De Angelis, F. First-Principles Modeling of Mixed Halide Organometal Perovskites for Photovoltaic Applications. *J. Phys. Chem. C* **2013**, *117*, 13902−13913.

(37) Preda, N.; Mihut, L.; Baibarac, M.; Baltog, I.; Lefrant, S. A Distinctive Signature in the Raman and Photoluminescence Spectra of Intercalated PbI_2. *J. Phys.: Condens. Matter* **2006**, *18*, 8899−8912.

(38) Wu, X.; Trinh, M. T.; Niesner, D.; Zhu, H.; Norman, Z.; Owen, J. S.; Yaffe, O.; Kudisch, B. J.; Zhu, X. Y. Trap States in Lead Iodide Perovskites. *J. Am. Chem. Soc.* **2015**, *137*, 2089−2096.

(39) Blancon, J. C.; Tsai, H.; Nie, W.; Stoumpos, C. C.; Pedesseau, L.; Katan, C.; Kepenekian, M.; Soe, C. M. M.; Appavoo, K.; Sfeir, M. Y.; et al. Extremely Efficient Internal Exciton Dissociation Through Edge States in Layered 2D Perovskites. *Science* **2017**, *355*, 1288−1291.

(40) Li, D. H.; Wang, G. M.; Cheng, H. C.; Chen, C. Y.; Wu, H.; Liu, Y.; Huang, Y.; Duan, X. F. Size-Dependent Phase Transition in Methylammonium Lead Iodide Perovskite Microplate Crystals. *Nat. Commun.* **2016**, *7*, 11330.

(41) Billing, D. G.; Lemmerer, A. Synthesis, Characterization and Phase Transitions in the Inorganic-Organic Layered Perovskite-Type Hybrids $[(C_nH_{2n+1}NH_3)_2PbI_4]$, n = 4, 5 and 6. *Acta Crystallogr., Sect. B: Struct. Sci.* **2007**, *63*, 735−747.

(42) Blancon, J. C.; Stier, A. V.; Tsai, H.; Nie, W.; Stoumpos, C. C.; Traore, B.; Pedesseau, L.; Kepenekian, M.; Katsutani, F.; Noe, G. T.; et al. Scaling Law for Excitons in 2D Perovskite Quantum Wells. *Nat. Commun.* **2018**, *9*, 2254.

(43) Stoumpos, C. C.; Soe, C. M. M.; Tsai, H.; Nie, W.; Blancon, J.-C.; Cao, D. H.; Liu, F.; Traoré, B.; Katan, C.; Even, J.; et al. High Members of the 2D Ruddlesden-Popper Halide Perovskites: Synthesis, Optical Properties, and Solar Cells of $(CH_3(CH_2)_3NH_3)_2(CH_3NH_3)_4Pb_5I_{16}$. *Chem.* **2017**, *2*, 427−440.